LANGMUIR TURBULENCE IN THE DECIMETER SOLAR FLARE ON MARCH 16, 2023.

© 2025 I. V. Kudryavtsev[a], *, N. E. Ovchinnikova[b], T. I. Kaltman[b]

[a]*A.F. Ioffe Institute of Physics and Technology, St. Petersburg, Russia*

[b]*St. Petersburg Branch of the Special Astrophysical Observatory of the Russian Academy of Sciences, St. Petersburg, Russia*

**e-mail: igor.koudriavtsev@mail.ioffe.ru*

Received February 24, 2025

Revised April 17, 2025

Accepted June 17, 2025

Abstract. We present the results of the analysis of the radio burst emission of March 16, 2023 for the period 07:45:24-07:45:30 UT measured with the RATAN-600 radio telescope in the frequency range of 1.0-1.6 GHz with high spectral resolution. It is hypothesized that the energy release in the region of bright coronal points was caused by the reclosure of magnetic fields, which was accompanied by electron acceleration and excitation of plasma waves. In this paper, the radio emission of the outburst is considered as a result of the merging of Langmuir waves, which forms transverse electromagnetic waves registered at RATAN-600. Langmuir wave spectra are obtained, allowing us to model the radio burst emission spectra for different time moments.

DOI: 10.31857/S00167940250707e6

1. INTRODUCTION

Coronal bright points (CBPs, see review [Madjarska, 2019]) with enhanced emission in the extreme ultraviolet and X-ray bands are a system of small-scale loops in the low corona.

CBP radio observations are an important tool to study coronal heating, particle acceleration, and magnetic field dynamics in small-scale solar structures. They complement data obtained in the X-ray and ultraviolet bands and help to investigate important solar physics questions such as coronal heating and energy released in CBPs.

In this work, we study the March 16, 2023 transient event 07:45:24-07:45:30 UT, associated with the CBP (Figs. 1, 2), in the decimeter range from observations on RATAN-600. The solar observations were carried out using a 1-3 GHz spectropolarimetric complex [Ripak et al., 2023] in two polarizations with a resolution of 4 MHz and a time resolution of 8 ms. After processing, the obtained temporal resolution of the spectrogram was 0.256 s.

In the range of 1.0-1.5 GHz, pulses of J-shape radio emission with a duration of 0.5 s and a width of 200-300 MHz were recorded. At this moment, the RATAN-600 directional pattern, while

scanning the Sun from west to east, passed through the area of the quiet Sun near the western part of the flocculus surrounding AO 13254 (Figs. 1, 2).

Fig. 1

The coincidence of the radio pulses in time with the dynamical evolution of coronal bright points (CBPs) recorded with AIA/SDO in the CUF (Fig. 2) indicates a physical connection between the radio burst and CBP activity. In addition, the narrow frequency range of the radio burst indicates a plasma mechanism for radio emission generation.

Fig. 2

The dynamics of the CBP emission has been recorded in all AIA lines, but only two are shown here: at 304 Å both points are clearly visible in one frame, and at 171 Å a system of loops lying above the CBPs and significantly overlapping them is observed. Nevertheless, the brightness variations of the points themselves are clearly reflected in the light profiles. The dynamics of the CBP emission in the 171 Å line indicates local heating of the plasma, and at the moment of radio emission registration at RATAN-600, the emission of one of the CBPs (in the blue box) sharply increases both at 171 Å and 304 Å, which may be related to magnetic reconnection. This indicates the simultaneous heating of the plasma and the possible development of Langmuir waves, the merging of which leads to radio emission. This pattern, which resembles a flare on a smaller scale, allows us to use CBP microbursts as an analog to study solar flare mechanisms.

The aim of this work is to determine the Langmuir spectrum that describes the spectra of a radio burst during its various stages. Under the assumption of a plasma mechanism of radio emission generation, modeling of the radio emission spectra and Langmuir wave spectra generating a given burst was performed.

2. MODELING OF LANGMUIR WAVE SPECTRA IN THE REGION OF THE SECOND PLASMA FREQUENCY AND RADIO BURST SPECTRA

Solar radio emission in the region of the double plasma frequency is known to be generated by the merger of Langmuir waves (see, for example, [Ginzburg and Zheleznyakov, 1958; Zheleznyakov and Zaitsev, 1970; Kaplan and Tsytovich, 1972; Zaitsev and Stepanov, 1983]). This radiation is characterized by its frequency spectrum [Willes et al., 1996; Kudryavtsev and Kaltman, 2021; Kudryavtsev et al., 2022] and directivity [Kudryavtsev and Kaltman, 2020], which depend on the spectra of Langmuir waves and their angular distribution.

The spectral power of radio emission generated by this mechanism in an inhomogeneous plasma of volume V can be written in the form

$$P_\omega(\omega,\vartheta,\varphi) = \int_V Q_\omega(\vec{r},\omega,\vartheta,\varphi)dV\ , \qquad (1)$$

where ϑ and φ are the polar and azimuthal angles of the wave vector of the electromagnetic wave **k**; $Q_{(\omega)}$ is the spectral energy density emitted by a unit volume of plasma, which is related to the spectral power of radiation by the wave number $Q_{\mathbf{k}}$ for different directions of radiation generation by the following relation (see, for example, the analogous formula for the isotropic case in [Tsytovich, 1971] and also [Willes et al., 1996]:

$$Q_\omega = k^2 Q_{\vec{k}} \frac{dk}{d\omega}\,, \tag{2}$$

Where, according to [Tsytovich, 1971],

$$Q_{\vec{k}} = \int Q_{\vec{k},\vec{k}_1,\vec{k}_2} \cdot W^l_{\vec{k}_1}(\vec{r}) \cdot W^l_{\vec{k}_2}(\vec{r}) d\vec{k}_1 d\vec{k}_2 \tag{3}$$

и

$$Q_{\vec{k},\vec{k}_1,\vec{k}_2} = \frac{\pi\omega\left(k_1^2 - k_2^2\right)^2 \left[\vec{k}_1\vec{k}_2\right]^2}{8mnk^2\omega_{pe}k_1^2k_2^2}\delta\left(\vec{k} - \vec{k}_1 - \vec{k}_2\right)\times \\ \delta\left(\sqrt{k^2c^2 + \omega_{pe}^2} - 2\omega_{pe} - \frac{3v_{Te}^2\left(k_1^2 + k_2^2\right)}{2\omega_{pe}}\right)\,, \tag{4}$$

where **k** and ω **are the** wave vector of the transverse electromagnetic wave and its frequency, ; , $\omega = \sqrt{k^2c^2 + \omega_{pe}^2}$ $v_{Te} = \sqrt{k_B T_e / m}$ k_B is the Boltzmann constant, T_e is the electronic temperature of the plasma, $\mathbf{k}_1$, $\mathbf{k}_2$ are the wave vectors of two Langmuir waves.

The energy density of plasma waves is determined by the expression:

$$W = \int W^l_{\vec{k}_1} d\vec{k}_1\,. \tag{5}$$

It follows from expressions (3) that the spectrum of radio emission generated by the merger of Langmuir plasmons will depend on the spectrum of Langmuir waves, which is discussed in detail in [Kudryavtsev and Kaltman, 2021; Kudryavtsev et al., 2022]. Figs. 1 and 2 show the radio burst spectra after subtraction of the background radiation for four consecutive time moments at 07:46:06 UTC; 07:46:08UTC; 07:46:09UTC; 07:46:10 UTC and the corresponding model spectra.

The considered burst moments are chosen so that the first two correspond to the growth phase, the third to the radio emission maximum, and the fourth to the emission decline.

When choosing the spectrum and angular distribution of Langmuir waves in the modeling, we will take into account that the angular distribution of plasmons primarily affects the directionality of radio emission generation (see, for example, [Kudryavtsev and Kaltman, 2020]), and the wave number distribution determines the spectrum of the generated radio emission [Kudryavtsev and Kaltman, 2021; Kudryavtsev et al, 2022]. In addition, it is worth noting that the induced scattering

of plasmons on thermal electrons results in a change in the direction of the wave vector predominantly nonlinear at angles ~ 180^0. In view of the above, the Langmuir wave spectrum was set in the modeling as:

$$W^l_{\vec{k}_{1,2}} = \begin{cases} A \cdot F(k) \cdot \cos^4(\vartheta) \; for \; \mathrm{k_{min}} \le \mathrm{k_{1,2}} \le \mathrm{k_{max}} \\ 0 \; for \, others \; k_{1,2} \end{cases}, \qquad (6)$$

where A is the normalization factor.

When choosing the type of function F(k), we, according to [Kudryavtsev and Kaltman, 2021; Kudryavtsev et al., 2022], will look for a function having a beginning and an end at wave numbers k_{min} and k_{max} and a maximum at k_0. These parameters will determine the beginning, maximum, and end of the radio emission spectrum.

The plasma wave spectra for the first three time moments (Fig. 1b and Fig. 2b, d) can be described by the expression:

$$F(k) = \begin{cases} \left(k_0/k\right)^{\gamma} \left((k-k_{\min})/(k_0-k_{\min})\right)^{\delta_1} \; for \; k_{\min} \le k \le k_0 \\ \dfrac{\left(k_0/k\right)^{\delta_2} - \left(k_0/k_{\max}\right)^{\delta_2}}{1-\left(k_0/k_{\max}\right)^{\delta_2}} \quad для \; k_0 \le k \le k_{\max} \\ 0 \quad for \, others \; k \end{cases} . \qquad (7)$$

parameters γ, δ_1, and $\delta_2$will determine the curvature of the radio burst spectrum. Since equation (1) is nonlinear with respect to the spectral energy density of Langmuir waves, we will find the parameters of the function F(k) by a fitting method, similar to [Kudryavtsev et al., 2022], so that the calculated radio emission spectrum satisfactorily describes the measured spectra. For the spectrum shown in Fig. 3a,b, δ_1= 0.7, δ_2= 0.25, γ = 1 and n_e= $3.7 \cdot 10^9 cm^{-3}$. Also in Fig. 3a,b shows an example of the choice of turbulence parameters. For the second instant (Fig. 3c, d): δ_1= 1, δ_2= 0.5, γ = 1 and n_e= $4.1 \cdot 10^9 cm^{-3}$. For the third instant (Fig. 3 e, f)): δ_1= 2, δ_2= 0.2, γ = 1.7 and n_e= $3.4 \cdot 10^9 cm^{-3}$.

For the fourth time instant, the Langmuir wave spectrum (Fig. 3h,g) can be described by the function c δ_1= 1.5, δ_2= 0.6 and n_e= $3.2 \cdot 10^9 cm^{-3}$:

$$F(k) = \begin{cases} \left((k-k_{\min})/(k_0-k_{\min})\right)^{\delta_1} для \; k_{\min} \le k \le k_0 \\ \dfrac{1-\left(k/k_{\max}\right)^{\delta_2}}{1-\left(k_0/k_{\max}\right)^{\delta_2}} \; for \; k_0 \le k \le k_{\max} \\ 0 \quad for \, others \; k \end{cases} , \qquad (8)$$

whereby, if F(k)>0.75 according to (6), then F(k) = 0.75.

On the spectra of Langmuir waves, one can distinguish region I, which can be interpreted as the region of generation of these waves, and region II, which is formed by nonlinear pumping of waves to the region of small wave numbers during induced scattering on plasma particles.

It should be noted here that the differences of the model spectra from the measured spectra in the 1.4-1.6 GHz range can be caused by thermal emission from the hot plasma. This burst is weak in intensity, and the given two intervals correspond to the growth phase. That is, the intensity of radio emission at these times is very low. As noted in the paper, this emission is also accompanied by the emission of heated plasma, registered in the ultraviolet range. However, this heated plasma generates thermal radiation in other ranges, including the radio band. In this case, this background radio emission varies in time as the temperature of the plasma changes. It should be noted that the emissivity of a completely black body according to the Rayleigh-Jeans formula grows at low frequencies as ν^2, where ν is the frequency of radio emission. Thus, the excess emission observed in the range 1.4-1.6 GHz, which is not reproduced by model calculations (Fig. 3a,c), may indicate an additional contribution of thermal radiation from the hot plasma.

3. CONCLUSION

1) The study of radio emission spectra in the region of the second plasma frequency allows us to diagnose plasma turbulence of the emitting region. For the March 16 event 2023 values of plasma electron concentration and plasma wave spectra have been found to describe the measured radio emission spectra.

2) Nonlinear Langmuir scattering leads to wave pumping in the region of small wave numbers, which is confirmed by modeling of plasma and electromagnetic wave spectra.

3) The unique combination of high sensitivity, high spectral and temporal resolutions of the RATAN-600 decimeter complex allows to study in detail the dynamics of the solar atmosphere and particle acceleration processes, including weak bursts and fine structures in radio emission.

ACKNOWLEDGEMENTS

The authors thank A.M. Ripak, V.M. Bogod, and M.K. Lebedev for the opportunity to use new data from the RATAN-600 solar complex obtained with the high-resolution decimeter-band radiometer.

The authors also thank the AIA project team (SDO) for the opportunity to use the data obtained with this instrument.

FUNDING

The work of I.V. Kudryavtsev was performed within the framework of the state assignment of A.F. Ioffe Federal Institute of Physics and Technology. The work of N.E. Ovchinnikova and T.I. Kaltman was performed within the framework of the state assignment of the SAO RAS, approved by the Ministry of Science and Higher Education of the Russian Federation.

Observations on the telescopes of SAO RAS are supported by the Ministry of Science and Higher Education of the Russian Federation. Upgrading of the instrumentation base is carried out within the framework of the national project "Science and Universities".

CONFLICT OF INTERESTS

The authors declare that they have no conflict of interest.

REFERENCES

1. *Ginzburg V.L. and Zheleznyakov V.V.* Possible mechanism of sporadic radio emission from the Sun (Radiation in isotropic plasma)//Astronomical Journal, V. 35, P. 694-712. 1958
2. *Zheleznyakov V.V., Zaitsev V.V.* On the theory of solar radio emission bursts of type III // Astronomical Journal, V. 47, No. 1, P.60-75. 1970
3. *Kaplan S.A., Tsytovich V.N.* Plasma Astrophysics. Moscow: Nauka. 440 p. 1972
4. *Ripak A.M., Bogod V.M., Grenkov S.A., Lebedev M.K.* Noise-resistant decimeter range radiometer for the RATAN-600 radio telescope // Astrophysical Bulletin, V. 78, P. 657-669, 2023
5. *Tsytovich V.N.* Theory of turbulent plasma. Moscow:Atomizdat. 424 p. 1971
6. *Kudryavtsev I.V., Kaltman T.I., and M. Karlický.* Diagnostics of the dynamics of the Langmuir spectrum based on radio emission during the 12 March 2015 solar radio burst // A&A 665, A98, 2022
7. *Kudryavtsev I.V. and Kaltman T.I.* On the influence of Langmuir wave spectra on the spectra of electromagnetic waves generated in solar plasma with double plasma frequency // MNRAS. V. 503, pp. 5740–5745. 2021
8. *Kudryavtsev I.V. and Kaltman T.I.* Influence of the Angular Distribution of Langmuir Waves on the Directivity of Radio Emission at Double Plasma Frequency // G&A. V. 60. № 8. P. 1122-1125. 2020
9. *Madjarska M.S.* Coronal bright points // Living Reviews in Solar Physics, Vol. 16, Issue 1, article id. 2, 79 pp., 2019
10. *Zaitsev V.V. and Stepanov A.V.* The plasma radiation of flare kernels // Solar Physics. V.88. P. 297-313. 1983.
11. *Willes A.J., Robinson P.A., Melrose D.B.* Second harmonic electromagnetic emission via Langmuir wave coalescence // Physics of Plasmas. V.3. pp.149-159. 1996

FIGURE CAPTIONS

Fig. 1. Spectrogram of the Sun's radio emission in the 1-3 GHz region for a section of the Sun with CBP, combined with the corresponding section of the nearest time frame AIA 304 Å, rotated according to the position angle of the RATAN-600 diagram.

Fig. 2. Emission of two coronal bright points (CBPs) from SDO/AIA data.

Top row - images: on the left, the southwestern part of the Sun in the 171 Å line; in the center and on the right, enlarged slices covering part of the flocculus of AO 13254 and both CBPs in the 171 Å and 304 Å lines. The red and blue boxes highlight the regions around the corresponding CBPs.

Bottom row - light curves of the CBPs in the 171 Å and 304 Å lines, normalized to unity by the maximum value. The color of the curves corresponds to the color of the frames in the images above; the integration of the emission was performed inside the indicated frames. The black vertical line indicates the moment of radio burst registration at RATAN-600.

Fig. 3. Measured and model radio emission spectra (a, c, e, g,; J on the vertical axis denotes the intensity in relative units) and the corresponding Langmuir wave spectra (b, d, f, h). At $T_e = 10^6$K for an observation angle of 90° (see Kudryavtsev and Kaltman, 2020).

(a, b) – $n_e = 3.7 \cdot 10^9 cm^{-3}$; $k_{min} = \omega_e/(15V_{Te})$; $k_{max} = \omega_e/(1.8V_{Te})$; для кривых 2–4 значение $k_0 = \omega_e/(3.35V_{Te})$; $k_0 = \omega_e/(3V_{Te})$; $k_0 = \omega_e/(2.9V_{Te})$ соответственно.

(c, d) – $n_e = 4.1 \cdot 10^9 cm^{-3}$; $k_{min} = \omega_e/(20V_{Te})$; $k_{max} = \omega_e/(2.4V_{Te})$; $k_0 = \omega_e/(3.9V_{Te})$;

(e, f) – $n_e = 3.4 \cdot 10^9 cm^{-3}$; $k_{min} = \omega_e/(25V_{Te})$; $k_{max} = \omega_e/(1.55V_{Te})$; $k_0 = \omega_e/(2.7V_{Te})$;

(g, h) – $n_e = 3.2 \cdot 10^9 cm^{-3}$; $k_{min} = \omega_e/(60V_{Te})$; $k_{max} = \omega_e/(1.7V_{Te})$; $k_0 = \omega_e/(2.8V_{Te})$.

The figures I and II highlight the regions of plasma wave generation and nonlinear "pumping" to the region of small wave numbers.

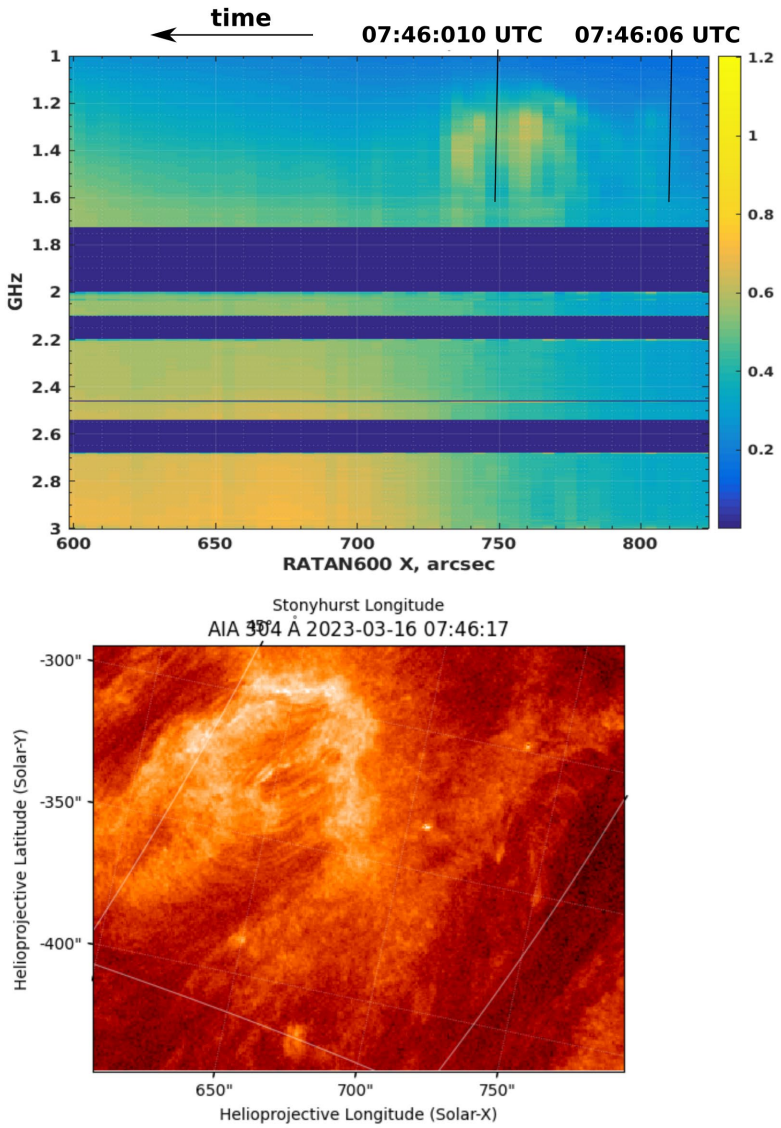
time
07:46:010 UTC
07:46:06 UTC
GHz
RATAN600 X, arcsec
Stonyhurst Longitude
AIA 304 Å 2023-03-16 07:46:17
Helioprojective Latitude (Solar-Y)
Helioprojective Longitude (Solar-X)

Fig. 1.

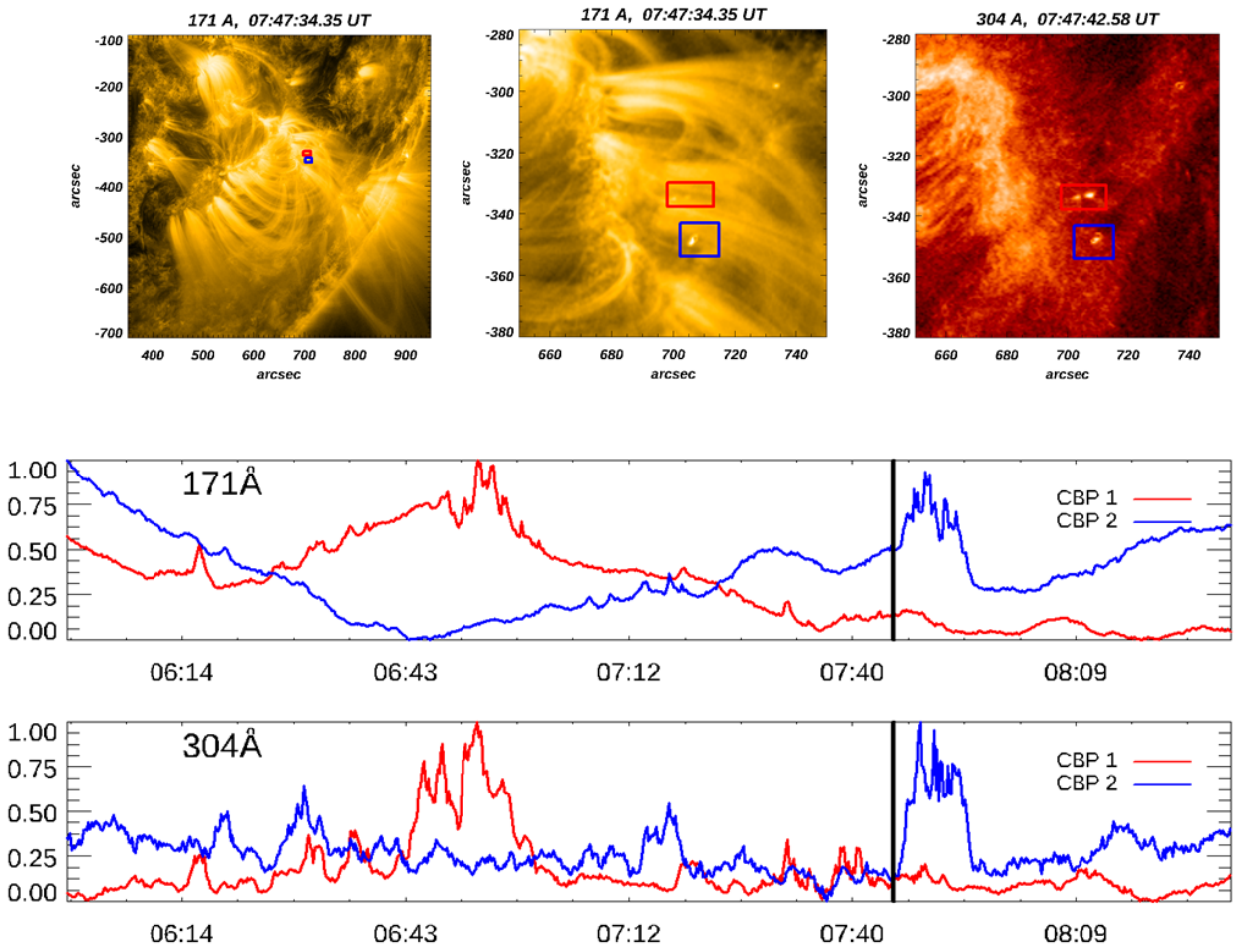
171 A, 07:47:34.35 UT
171 A, 07:47:34.35 UT
304 A, 07:47:42.58 UT
arcsec
171Å
304Å
CBP 1
CBP 2
06:14
06:43
07:12
07:40
08:09

Fig. 2.

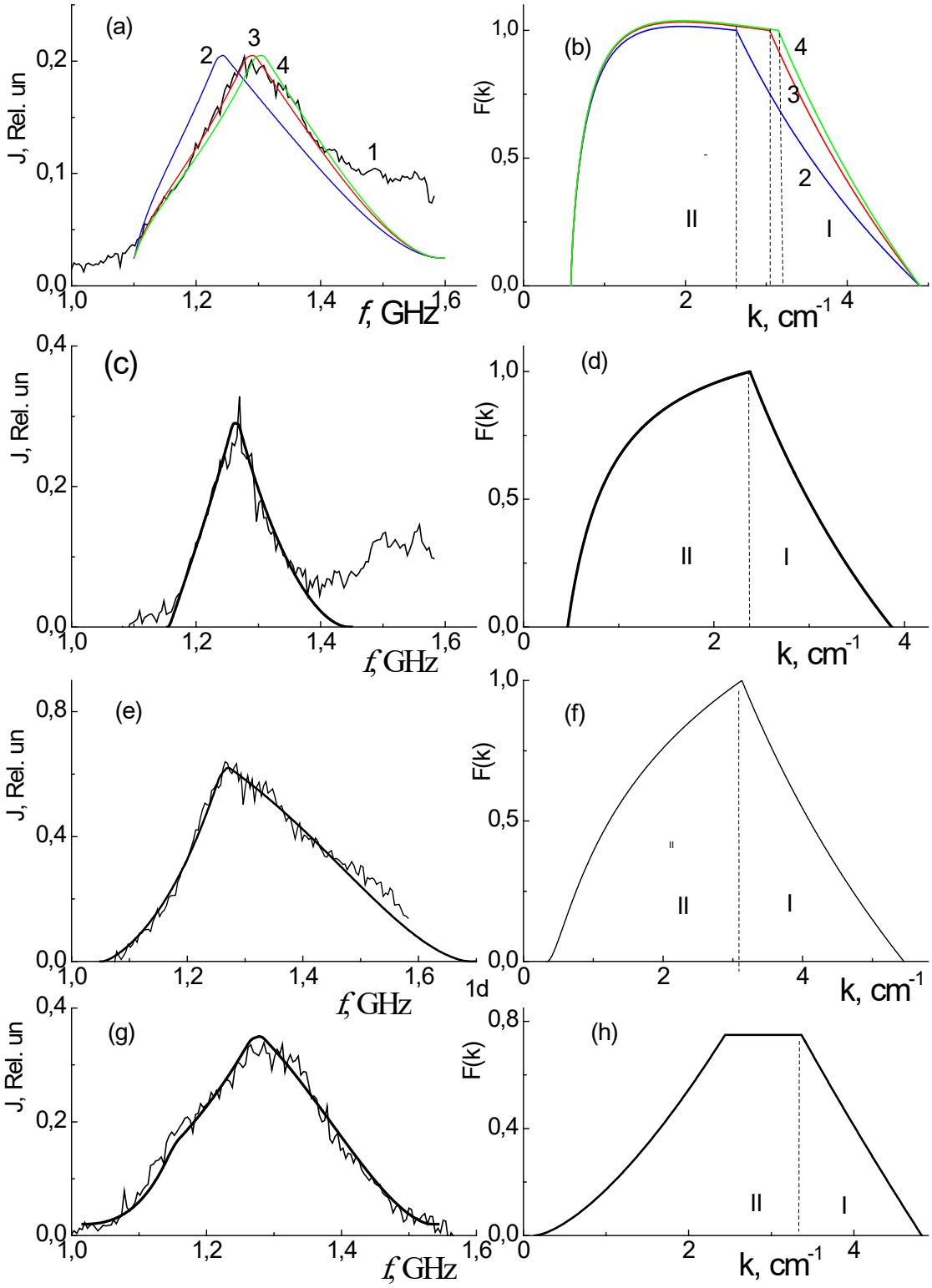

Fig. 3.